Pergamon

J. Quant. Spectrosc. Radiat. Transfer Vol. 52, No. 2, pp. 167–177, 1994
0022-4073(94)E0046-9

0022-4073/94 $7.00 + 0.00

LASER OPTOGALVANIC WAVELENGTH CALIBRATION WITH A COMMERCIAL HOLLOW CATHODE IRON–NEON DISCHARGE LAMP

XINMING ZHU, ABDULLAHI H. NUR, and PRABHAKAR MISRA†
Laser Spectroscopy Laboratory, Department of Physics and Astronomy, Howard University, Washington, DC 20059, U.S.A.

(Received 17 November 1993)

Abstract—351 optogalvanic transitions have been observed in the 337–598 nm wavelength region using an iron–neon hollow cathode discharge lamp and a pulsed tunable dye laser. 223 of these have been identified as transitions associated with neon energy levels. These optogalvanic transitions have allowed, in conjunction with interference fringes recorded concomitantly with an etalon, the calibration of the dye laser wavelength with 0.3 cm^{-1} accuracy.

INTRODUCTION

Wavelength calibration of tunable lasers is important in experimental laser spectroscopy. An iodine absorption cell can be used for precise calibration of the spectral region 500–675 nm in the visible, since a good atlas exists for that region.[1] However, in the blue and near u.v. regions of the electromagnetic spectrum, there is a paucity of suitable species for wavelength calibration of tunable lasers. Tellurium has been employed by Miller.[2] However, its spectral atlas is not easily accessible. The optogalvanic (OG) effect provides a good solution for wavelength calibration inadequacies in the visible and near u.v. regions of the electromagnetic spectrum.

The OG effect, discovered by Penning[3] in 1928, is the impedance change of a neon discharge tube when illuminated by a second neon discharge tube. In 1976, Green et al[4] observed the OG effect with a tunable dye laser and measured the changes in voltage across a low-pressure gas discharge tube irradiated by a laser beam that was tuned to the wavelength of transition of a species present in the discharge. These authors reported optogalvanic signals for transitions involving lithium, sodium, calcium, barium, uranium, neon, and helium. It was pointed out[4] that the OG effect might have significant impact in optical spectroscopy and other areas of applied physics and chemistry. Extensive work has since been carried out to understand the OG effect in some detail and to use it in laser spectroscopy. Precise wavelength calibration of tunable lasers is an important application of the OG effect.

OG lines have been observed in case of various species sputtered from hollow cathodes[4–9] and from fill gases such as neon and argon.[4,10–19] A larger discharge current (>20 mA) is needed for exciting OG transitions associated with species sputtered from cathodes as compared to the signal from the gas atoms. Uranium, for example, is a good candidate for producing the OG effect, because it is an excellent wavelength standard. In addition, uranium gives rise to spectral lines that are narrow and do not possess hyperfine structure over a wide spectral region extending from the infrared to the ultraviolet. However, the OG signals arising from discharge gases are usually much stronger than those from cathode elements. OG transitions from argon have been observed in the wavelength regions 367–422 nm,[19] 415–670 nm,[15] 425–700 nm,[14] 420–740 nm,[16] 555–575 nm,[17] 727–772 nm,[13] 360–740 nm,[18] 2440–2780 nm.[11] OG signals with commercial neon lamps, which are

†To whom all correspondence should be addressed.

extensively used as spectral light sources, have been reported in the 540–750 nm[4,10,13,20] and 2440–2780 nm[11] regions. However, neon transitions do not seem to have been reported in the blue and near u.v. regions. It has been pointed out[14] that it is difficult to obtain OG resonances with neon in wavelength regimes shorter than 580 nm owing to low oscillator strengths of the resonances.

In a series of measurements we have recently observed laser-assisted OG signals with neon in the 337–598 nm region by employing a commercial iron–neon hollow cathode lamp. 223 of these OG transitions have been identified to be associated with neon energy levels. Surprisingly, we have found that there are more OG lines of neon in the near-u.v. region than in the yellow and red regions, and interestingly the OG signals in wavelength regimes shorter than 360 nm are very strong. Interference fringes from two surfaces of an etalon were also recorded simultaneously to determine an unknown transition wavelength between two neon transitions. The optogalvanic lines reported here should be useful for accurate wavelength calibration of tunable lasers in high-resolution laser spectroscopy.

EXPERIMENTAL

Figure 1 shows the experimental arrangement for the OG wavelength calibration in our laser-induced fluorescence investigations. A dye laser (DL) is pumped by an excimer laser (EL) running at 10 Hz. The output beam has a pulse duration of about 20 nsec. and a nominal linewidth of 0.07 cm^{-1} without any intracavity etalon. The tuning range 336–600 nm was covered by the following Exciton laser dyes: P-Terphenyl, TMQ, BPBD, Exalite 376, Exalite 389, Exalite 398, DPS, Bis-MSB, Coumarin 440, Coumarin 460, Coumarin 480, Coumarin 500, Coumarin 540 and Rhodamine 590. An uncoated quartz wedge (WD) was inserted in the optical path of the primary beam to pick off two weak beams (each about 5% of the primary pulse energy). One of the beams (unfocussed and of typical pulse energy 100 μJ) enters the cathode of a commercial iron–neon hollow cathode lamp through a 1 mm diameter aperture. The second beam traverses a negative lens (NL) and illuminates an uncoated, parallel-faced 6 mm thick quartz disk at a small angle of incidence (1–2 deg) which serves as a low-finesse etalon (ET). The interference pattern, generated by the reflection beams from the front and rear surfaces of the disk, is recorded after passage through a pinhole aperture (AP) by a photodiode (PD).

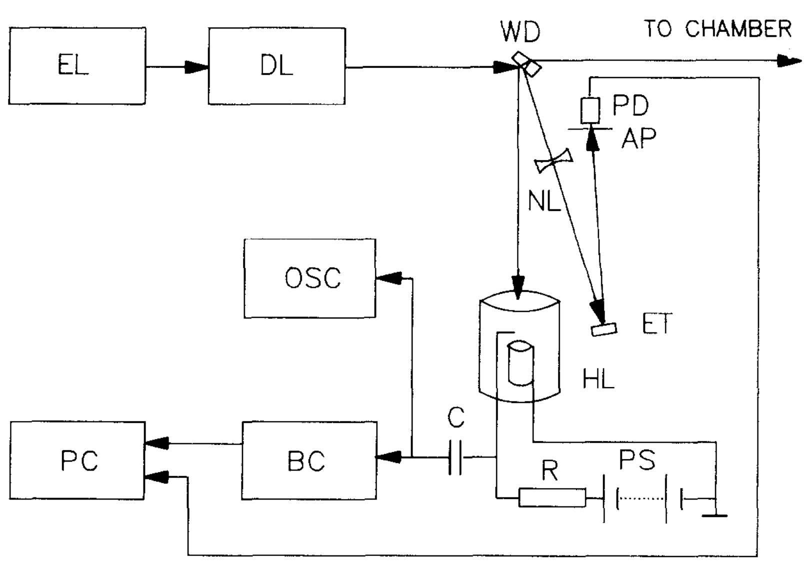

Fig. 1. Experimental arrangement for laser optogalvanic wavelength calibration. EL = Excimer Laser, DL = Dye Laser, WD = Wedge, PD = Photodiode, AP = Aperture, NL = Negative Lens, OSC = Oscilloscope, HL = Hollow Cathode Discharge Lamp, PC = Personal Computer, BC = Boxar Averager, C = Capacitor, R = Resistor, PS = Power Supply.

A high-voltage power supply (PS) and a ballast resistor (R) of 20 kΩ were used for the iron–neon lamp. The discharge current was set at 1 mA and the voltage across the lamp was 160 V. When the laser pulse is resonantly absorbed by the discharge medium, the voltage across the lamp varies, and these variations are coupled via a 0.05 μF capacitor to a boxcar integrator (BC). The temporal evolution of the signal was recorded by a digital oscilloscope. The outputs of the boxcar and the photodiode were recorded with a microcomputer-aided data acquisition system. The OG signal and the interference fringes were recorded simultaneously as illustrated in Fig. 2.

RESULTS AND DISCUSSION

351 OG transitions have been recorded in the 336.99–597.55 nm wavelength region and are listed in Table 1. 223 of these lines have been identified as due to neon. The assignments of the transitions and the associated emission intensities follow Ref. 21. The OG transitions have been identified according to the J–L coupling scheme of Racah.[22] The electronic configuration of the neon ion is $1s^22s^22p^5$ with the spectral terms $^2P^0_{1.5}$ and $^2P^0_{0.5}$. When a 3s electron is added to the $^2P^0_{1.5}$ configuration, the generated energy levels are designated 3s [1.5]^{0}1 and 3s [1.5]^{0}2. The number 1.5 within the parentheses represents one of the vector sums of the ionic J and the l value of the added electron ($l = 0$ for an s electron) and the superscript 0 indicates odd parity. The number on the right of the parenthesis is the total J value; it is the vectorial sum of the ionic J and the spin of the added 3s electron. Similarly, if a 3p electron is added to the ionic term $^2P^0_{1.5}$, the generated energy levels are 3p′[0.5]0, 3p′[0.5]1, 3p′[1.5]1 and 3p′[1.5]2, where the prime indicates that the level is generated from the $J = 0.5$ ionic level. 128 OG lines have been recorded and tabulated in Table 1, but have not been assigned. These are confined mainly to the spectral region 361.5–427.6 nm. These transitions are probably due to weak emission lines not listed in the neon atlas. Because the current in the discharge lamp was only 1 mA, we did not expect to observe any iron transitions. The time evolution of the OG signals was recorded by a digital oscilloscope. The amplitudes of the signals were varied from 10 mV to 2 V and weaker lines were not recorded. The waveforms had different shapes for the various kinds of observed transitions and depended on the magnitude of the discharge current. Most observed pulses had an initial negative peak, rose to cross the base line and became positive. Figure 3(a), (b), and (c) shows the OG signal waveforms for three distinct transitions at wavelengths (in air) 3510.721, 3515.190, and 3520.471 Å, respectively. Each curve was an average over 1000 events. All the three waveforms were recorded with the discharge current maintained at 0.5 mA and the laser pulse energy at 20 μJ. However, it can be

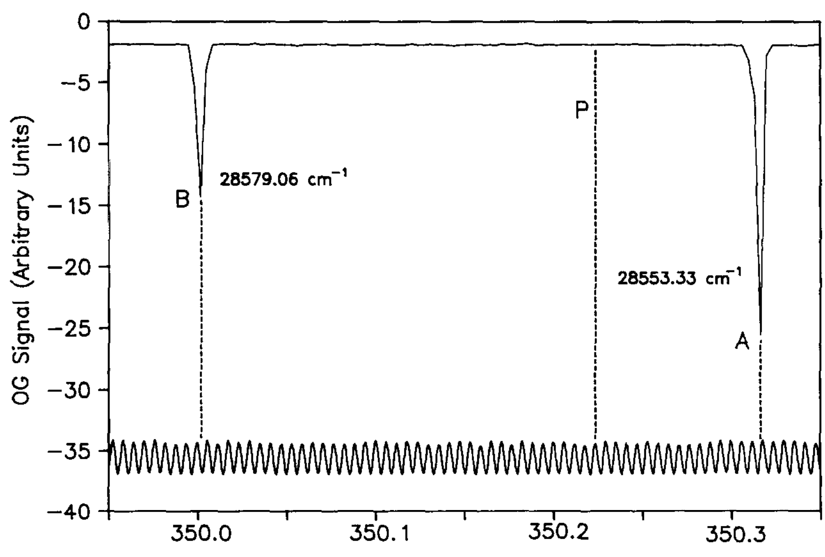

Fig. 2. Sample optogalvanic spectrum of neon (top) and the interference pattern of the etalon (bottom) around 350 nm.

Table 1. Optogalvanic neon transitions in the 3369–5980 Å region.

Wavelength in Air(Å)	Intensity of Emission	Ne Transition	OG Signal Intensity(mV)	Laser Energy (μJ)
3369.9069	700	3s [1.5]°2 — 4p'[0.5]1	1500	50
3375.6489	50	3s [1.5]°2 — 4p'[1.5]1	100	55
3417.9031	500	3s [1.5]°1 — 4p'[1.5]2	700	70
3418.007	50	3s [1.5]°1 — 4p'[0.5]1	400	60
3423.9120	50	3s [1.5]°1 — 4p'[1.5]1	200	60
3447.7022	200	3s [1.5]°2 — 4p [1.5]2	20	45
3450.7641	50	3s [1.5]°2 — 4p [1.5]1	1300	40
3454.1942	100	3s [1.5]°1 — 4p [0.5]0	600	20
3460.5235	100	3s'[0.5]°0 — 4p'[0.5]1	600	25
3464.3385	100	3s [1.5]°2 — 4p [2.5]2	1000	25
3466.5781	200	3s'[0.5]°0 — 4p'[1.5]1	1000	30
3472.5706	500	3s [1.5]°2 — 4p [2.5]3	300	30
3498.0632	100	3s [1.5]°1 — 4p [1.5]2	150	35
3501.2154	200	3s [1.5]°1 — 4p [1.5]1	200	35
3510.7207	50	3s [1.5]°2 — 4p [0.5]1	800	40
3515.1900	200	3s [1.5]°1 — 4p [2.5]2	150	40
3520.4714	1000	3s'[0.5]°1 — 4p'[0.5]0	50	45
3593.5263	500	3s'[0.5]°1 — 4p'[1.5]2	25	50
3600.1694	100	3s'[0.5]°1 — 4p'[1.5]1	15	45
3609.1787	50	3s'[0.5]°0 — 4p [0.5]1	150	50
3614.23			10	50
3621.87			5	55
3626.19			10	55
3628.82			25	60
3633.6643	100	3s'[0.5]°1 — 4p [0.5]0	35	80
3682.2421	100	3s'[0.5]°1 — 4p [1.5]2	25	50
3685.02			22	50
3685.7351	100	3s'[0.5]°1 — 4p [1.5]1	28	50
3701.2247	40	3s'[0.5]°1 — 4p [2.5]2'	35	70
3754.2148	50	3s'[0.5]°1 — 4p [0.5]1	18	60
3829.77			10	45
3862.57			15	120
3876.00			15	130
3880.39			5	130
3893.02			20	130
3915.21			20	110
3922.25			6	90
3922.96			7	90
3924.57			7	90
3927.18			8	80
3927.31			8	80
3933.58			8	80
3942.19			18	80
3943.33			34	60
3946.26			20	100
3947.98			14	100
3952.70			22	100
3953.58			14	100
3954.00			10	100
3954.72			16	100
3960.45			22	110
3962.92			18	110
3969.66			24	120
3969.78			25	120
3972.59			9	120
3972.80			20	120
3981.16			23	130
3981.33			23	130
3984.065	2	3p [0.5] 1 — 9d'[1.5]°1	22	130
3984.253	7	3p [0.5] 1 — 9d'[2.5]°2	35	130
3985.12			12	130
3995.50			28	120
3995.721	1	3p [0.5] 1 — 13d [0.5]°1	27	120
3998.594	1	3p [0.5] 1 — 10s'[0.5]°1	34	120
3999.263	1	3p [0.5] 1 — 10s'[0.5]°0	14	120
4000.24			14	120
4000.44			24	120
4013.752	1	3p [0.5] 1 — 12d [1.5]°2	28	120
4013.995	2	3p [0.5] 1 — 12s [0.5]°1	25	110
4020.015	2	3p [0.5] 1 — 13s [1.5]°2	20	100
4037.262	5	3p [0.5] 1 — 11d [1.5]°2	20	100

continued opposite

Table 1—*continued.*

Wavelength in Air(Å)	Intensity of Emission	Ne Transition	OG Signal Intensity(mV)	Laser Energy (μJ)
4037.615	15	3p [0.5] 1 — 11d [0.5]^{o}1	20	100
4037.696	5	3p [0.5] 1 — 11d [0.5]^{o}0	10	100
4042.327	10	3p [0.5] 1 — 8d'[1.5]^{o}1	20	110
4042.642	50	3p [0.5] 1 — 8d'[2.5]^{o}2	25	110
4045.04			10	110
4045.662	2	3p [0.5] 1 — 12s [1.5]^{o}2	12	110
4064.036	50	3p [0.5] 1 — 9s'[0.5]^{o}1	15	110
4064.829	15	3p [0.5] 1 — 9s'[0.5]^{o}0	10	120
4068.835	30	3p [0.5] 1 — 10d [1.5]^{o}2	20	120
4069.243	30	3p [0.5] 1 — 10d [0.5]^{o}1	20	120
4069.389	5	3p [0.5] 1 — 10d [0.5]^{o}0	13	120
4079.359	2	3p [0.5] 1 — 11s [1.5]^{o}1	9	110
4080.148	50	3p [0.5] 1 — 11s [1.5]^{o}2	15	110
4087.82			8	110
4097.79			8	100
4111.84			10	90
4112.100	15	3p [0.5] 1 — 9d [1.5]^{o}2	12	80
4112.694	20	3p [0.5] 1 — 9d [0.5]^{o}1	12	80
4112.885	10	3p [0.5] 1 — 9d [0.5]^{o}0	8	80
4125.14			8	70
4126.941	2	3p [0.5] 1 — 10s [1.5]^{o}1	12	50
4128.072	30	3p [0.5] 1 — 10s [1.5]^{o}2	24	50
4130.512	20	3p [0.5] 1 — 7d'[1.5]^{o}1	15	60
4131.054	70	3p [0.5] 1 — 7d'[2.5]^{o}2	20	70
4144.51			17	90
4148.81			10	100
4149.50			10	100
4151.37			15	100
4152.18			12	100
4154.31			25	110
4155.22			20	110
4157.65			30	110
4158.70			22	110
4160.82			10	110
4161.51			30	110
4162.69			26	110
4164.802	50	3p [0.5] 1 — 8s'[0.5]^{o}1	20	110
4166.091	30	3p [0.5] 1 — 8s'[0.5]^{o}0	40	120
4167.32			30	120
4169.69			20	120
4171.08			40	120
4171.74			10	120
4172.74			35	120
4173.966	2	3p [0.5] 1 — 8d [1.5]^{o}1	15	120
4174.369	70	3p [0.5] 1 — 8d [1.5]^{o}2	28	120
4175.223	60	3p [0.5] 1 — 8d [0.5]^{o}1	22	120
4175.488	40	3p [0.5] 1 — 8d [0.5]^{o}0	20	120
4176.44			10	130
4177.16			40	130
4179.11			35	130
4180.37			10	130
4182.03			10	130
4183.39			10	130
4184.36			45	130
4186.75			45	130
4190.65			15	130
4191.80			10	130
4193.00			50	130
4195.15			15	140
4195.78			40	140
4196.415	15	3p [0.5] 1 — 9s [1.5]^{o}1	25	140
4198.099	70	3p [0.5] 1 — 9s [1.5]^{o}2	22	140
4200.40			18	140
4201.95			10	140
4203.270	2	3p [2.5] 2 — 10d'[2.5]^{o}3	60	140
4203.43			50	140
4206.43			16	140
4206.83			40	140

continued overleaf

Table 1—*continued.*

Wavelength in Air(Å)	Intensity of Emission	Ne Transition	OG Signal Intensity(mV)	Laser Energy (μJ)
4208.30			10	140
4208.47			10	140
4210.58			10	140
4213.80			20	140
4214.87			10	140
4216.04			50	140
4216.24			55	140
4220.61			40	140
4222.58			20	140
4225.31			14	140
4230.78			15	140
4232.07			40	140
4232.33			50	140
4233.17			32	140
4236.47			15	140
4236.70			10	140
4237.80			40	130
4246.24			20	130
4249.538	2	3p [2.5] 2 — 9d'[2.5]°2	20	130
4250.28			15	130
4252.418	2	3p [2.5] 3 — 12d [2.5]°3	45	130
4252.775	2	3p [2.5] 3 — 12d [3.5]°4	50	130
4256.498	2	3p [1.5] 1 — 10d'[2.5]°2	12	130
4256.99			13	120
4259.40			10	120
4259.77			40	120
4261.78			10	120
4262.23			15	120
4262.479	2	3p [2.5] 2 — 13d [3.5]°3	20	120
4265.89			10	120
4267.724	5	3p [0.5] 1 — 7d [1.5]°1	20	120
4268.009	70	3p [0.5] 1 — 7d [1.5]°2	35	120
4268.30			15	120
4269.724	70	3p [0.5] 1 — 7d [0.5]°1	20	120
4270.267	50	3p [0.5] 1 — 7d [0.5]°0	15	120
4271.19			12	110
4274.656	50	3p [0.5] 1 — 6d'[1.5]°1	25	110
4275.5598	70	3p [0.5] 1 — 6d'[1.5]°2	25	110
4278.850	5	3p [2.5] 3 — 11d [2.5]°3,2	45	110
4279.06			30	110
4279.279	15	3p [2.5] 3 — 11d [3.5]°4,3	45	110
4282.84			12	110
4283.242	10	3p [2.5] 2 — 12d [3.5]°3	20	100
4287.03			10	100
4288.541	5	3p [2.5] 3 — 12s [1.5]°2	30	100
4288.93			10	90
4289.94			12	90
4290.40			10	90
4291.976	2	3p [1.5] 2 — 10d'[2.5]°2,3	20	90
4292.46			12	80
4293.09			10	80
4303.02			10	70
4303.955	5	3p [1.5] 1 — 9d'[2.5]°2	10	70
4306.2625	70	3p [0.5] 1 — 8s [1.5]°2	20	100
4309.10			18	100
4310.130	2	3p [2.5] 2 — 11d [3.5]°3	20	110
4314.110	1	3p [2.5] 3 — 10d [2.5]°3	45	110
4314.695	30	3p [2.5] 3 — 10d [3.5]°4,3	45	110
4316.008	15	3p [2.5] 2 — 8d'[2.5]°3,2	20	110
4327.265	10	3p [2.5] 3 — 11s [1.5]°2	34	120
4340.418	2	3p [2.5] 2 — 9s'[0.5]°1	20	120
4346.036	15	3p [2.5] 2 — 10d [3.5]°3	19	130
4362.690	30	3p [2.5] 3 — 9d [2.5]°3	25	150
4363.228	2	3p [2.5] 3 — 9d [1.5]°2	25	150
4363.524	70	3p [2.5] 3 — 9d [3.5]°4	40	150
4374.997	2	{3p [1.5] 2 — 12d [2.5]°3 {3p [1.5] 1 — 12s [1.5]°1	20	160
4381.220	30	3p [2.5] 3 — 10s [1.5]°2	35	160
4395.69			18	160
4422.5205	300	3p [0.5] 1 — 6d [1.5]°2	20	160

continued opposite

Table 1–*continued.*

Wavelength in Air(Å)	Intensity of Emission	Ne Transition	OG Signal Intensity(mV)	Laser Energy (μJ)
4424.8096	300	3p [0.5] 1 — 6d [0.5]^{o}1	20	160
4432.526	20	3p [2.5] 3 — 8d [2.5]^{o}3	30	160
4433.398	10	3p [2.5] 3 — 8d [1.5]^{o}2	22	160
4433.7239	70	3p [2.5] 3 — 8d [3.5]^{o}4	35	160
4460.175	100	3p [2.5] 3 — 9s [1.5]^{o}2	25	150
4491.838	50	3p [1.5] 2 — 5d [2.5]^{o}2,3	20	130
4517.736	100	3p'[1.5] 2 — 8d'[2.5]^{o}3	12	120
4536.312	150	3p [0.5] 1 — 5d'[1.5]^{o}1	15	100
4537.683	300	3p [0.5] 1 — 5d'[1.5]^{o}2	15	100
4537.7545	1000	3p [0.5] 1 — 5d'[2.5]^{o}2	18	110
4538.293	300	3p [2.5] 3 — 7d [2.5]^{o}3	20	110
4539.168	50	3p [2.5] 3 — 7d [1.5]^{o}2	15	110
4540.380	50	3p [2.5] 3 — 7d [3.5]^{o}4	35	110
4547.218	10	3p [2.5] 3 — 6d [2.5]^{o}3	12	120
4565.888	60	3p [1.5] 2 — 8d [2.5]^{o}3	12	130
4567.139	15	3p [1.5] 2 — 8d [3.5]^{o}3	10	130
4573.066	5	3p [2.5] 2 — 7d [2.5]^{o}2	13	130
4573.557	50	3p [2.5] 2 — 7d [1.5]^{o}1	10	130
4573.93			10	130
4575.0620	300	3p [2.5] 2 — 7d [3.5]^{o}3	15	130
4582.035	150	3p [2.5] 2 — 6d'[2.5]^{o}3	18	140
4582.4521	150	3p [2.5] 3 — 8s [1.5]^{o}2	24	140
4596.54			10	140
4604.095	15	3p'[1.5] 2 — 9d [2.5]^{o}3	10	140
4609.910	150	3p'[1.5] 1 — 7d'[1.5]^{o}2	10	140
4614.391	100	3p [2.5] 2 — 8s [1.5]^{o}1	10	140
4617.837	70	3p [2.5] 2 — 8s [1.5]^{o}2	10	140
4628.3113	150	3p'[1.5] 2 — 7d'[2.5]^{o}2,3	12	130
4636.125	70	3p [1.5] 1 — 7d [2.5]^{o}2	10	130
4645.4180	300	3p [1.5] 1 — 6d'[2.5]^{o}2	7	130
4656.3936	300	3p [0.5] 1 — 6s'[0.5]^{o}1	12	120
4661.1054	150	3p [0.5] 1 — 6s'[0.5]^{o}0	11	120
4679.135	150	3p [1.5] 2 — 7d [1.5]^{o}2	12	100
4680.363	100	3p [1.5] 2 — 7d [3.5]^{o}3	11	100
4687.6724	100	3p [1.5] 2 — 6d'[2.5]^{o}3	13	90
4702.526	150	3p [0.5] 1 — 5d [1.5]^{o}1	14	80
4704.3949	1500	3p [0.5] 1 — 5d [1.5]^{o}2	20	80
4708.8619	1200	3p [0.5] 1 — 5d [0.5]^{o}1	18	70
4710.0669	1000	3p'[0.5] 1 — 5d [0.5]^{o}0	13	60
4712.066	1000	3p [2.5] 3 — 6d [2.5]^{o}3	30	90
4714.336	70	3p [2.5] 3 — 6d [1.5]^{o}2	24	90
4715.3466	1500	3p [2.5] 3 — 6d [3.5]^{o}4	34	90
4721.536	70	3p [1.5] 2 — 8s [1.5]^{o}1	9	100
4723.810	70	{3p [0.5] 0 — 9s [1.5]^{o}1 3p'[0.5] 1 — 8d [0.5]^{o}1	10	100
4749.5754	300	3p [2.5] 2 — 6d [2.5]^{o}2	14	110
4750.686	30	3p [2.5] 2 — 6d [1.5]^{o}1	30	110
4751.802	30	3p [2.5] 2 — 6d [1.5]^{o}2	11	110
4752.7320	500	3p'[0.5] 2 — 6d [3.5]^{o}3	16	110
4758.728	150	3p [1.5] 2 — 7s'[0.5]^{o}1	8	110
4774.88			8	120
4774.94			8	120
4780.338	300	3p'[1.5] 1 — 7d [2.5]^{o}2	9	120
4788.9270	1000	3p [2.5] 3 — 7s [1.5]^{o}2	22	120
4789.600	100	3p'[1.5] 1 — 6d'[1.5]^{o}1	8	120
4790.218	500	3p'[1.5] 1 — 6d'[1.5]^{o}2	10	120
4799.41			8	110
4800.111	15	3p'[1.5] 2 — 7d [2.5]^{o}3	12	110
4802.363	10	3p'[1.5] 2 — 7d [3.5]^{o}3	8	110
4809.500	10	3p'[1.5] 2 — 6d'[1.5]^{o}1	8	110
4810.0640	150	3p'[1.5] 2 — 6d'[2.5]^{o}3	14	110
4810.634	100	3p'[1.5] 2 — 6d'[2.5]^{o}2	11	110
4810.84			8	110
4817.6386	300	3p [1.5] 1 — 6d [2.5]^{o}2	9	110
4818.789	150	3p [1.5] 1 — 6d [1.5]^{o}1	8	110
4819.937	70	3p [1.5] 1 — 6d [1.5]^{o}2	8	110
4821.9236	300	3p [2.5] 2 — 7s [1.5]^{o}1	10	100
4827.3444	1000	3p [0.5] 1 — 6s [1.5]^{o}1	10	100

continued overleaf

Table 1—*continued.*

Wavelength in Air(Å)	Intensity of Emission	Ne Transition	OG Signal Intensity(mV)	Laser Energy (μJ)
4837.3139	500	3p [0.5] 1 — 6s [1.5]°2	13	100
4842.941	50	3p'[0.5] 1 — 7d [1.5]°2	8	100
4849.530	30	3p'[1.5] 2 — 8s [1.5]°2	8	100
4852.6571	100	3p'[0.5] 1 — 6d'[2.5]°2	8	100
4859.604	15	3p [0.5] 0 — 8s [1.5]°1	8	90
4863.0800	100	3p [1.5] 2 — 6d [2.5]°3	13	90
4865.501	100	3p [1.5] 2 — 6d [1.5]°2	11	90
4866.476	80	3p [1.5] 2 — 6d [3.5]°3	10	90
4868.268	70	3p [1.5] 2 — 6d [0.5]°1	8	90
4884.9170	1000	{3p'[1.5] 2 — 7s'[0.5]°1	19	80
		{3p [2.5] 2 — 5d'[2.5]°3		80
4885.084	100	3p [2.5] 2 — 5d'[2.5]°2	10	80
4905.19			8	70
4927.48			10	50
4928.235	70	3p'[0.5] 1 — 7s'[0.5]°1	7	50
4939.0457	100	3p [1.5] 2 — 7s [1.5]°1	10	60
4944.9899	100	3p [1.5] 2 — 7s [1.5]°2	10	60
4955.382	150	3p [1.5] 1 — 5d'[1.5]°1	11	60
4957.0335	1000	3p [1.5] 1 — 5d'[1.5]°2	12	70
4973.538	100	3p'[1.5] 1 — 6d [2.5]°2	8	70
4974.760	50	3p'[1.5] 1 — 6d [1.5]°1	6	70
4994.10			8	90
4994.930	150	3p'[1.5] 2 — 6d [2.5]°3	9	90
4997.482	15	3p'[1.5] 2 — 6d [1.5]°2	8	90
4997.96			12	90
4998.502	10	3p'[1.5] 2 — 6d [3.5]°3	12	90
5005.1587	500	3p [1.5] 2 — 5d'[2.5]°3	10	100
5022.870	25	3p [2.5] 2 — 6s'[0.5]°1	8	100
5031.3504	250	3p [2.5] 3 — 5d [2.5]°3	23	100
5035.989	35	3p [2.5] 3 — 5d [1.5]°2	20	110
5037.7512	500	3p [2.5] 3 — 5d [3.5]°4	25	110
5074.201	35	3p [2.5] 2 — 5d [2.5]°2	12	110
5076.5816	35	3p [2.5] 2 — 5d [1.5]°1	10	110
5078.762	15	3p [2.5] 2 — 5d [1.5]°2	9	110
5080.3852	150	3p [2.5] 2 — 5d [3.5]°3	13	110
5083.968	25	3p [2.5] 2 — 5d [0.5]°1	8	120
5113.6724	75	3p [0.5] 1 — 4d [1.5]°1	12	120
5116.5032	150	3p [0.5] 1 — 4d'[1.5]°2	14	120
5117.011	35	3p [0.5] 1 — 4d'[2.5]°2	12	120
5122.257	150	3p'[1.5] 1 — 5d'[1.5]°2	9	120
5122.337	150	3p'[1.5] 1 — 5d'[2.5]°2	9	120
5129			8	110
5144.9384	500	3p'[1.5] 2 — 5d'[2.5]°3	13	110
5150.077	35	3p [1.5] 2 — 6s'[0.5]°1	8	110
5151.9610	75	3p [1.5] 1 — 5d [2.5]°2	8	110
5154.4271	50	3p [1.5] 1 — 5d [1.5]°1	8	110
5156.667	50	3p [1.5] 1 — 5d [1.5]°2	8	110
5188.6122	150	3p [2.5] 3 — 6s [1.5]°2	15	100
5193.1302	150	3p'[0.5] 1 — 5d'[1.5]°2	8	100
5193.2227	150	3p'[0.5] 1 — 5d'[2.5]°2	8	100
5203.8962	150	3p [1.5] 2 — 5d [2.5]°3	10	90
5208.8648	70	3p [1.5] 2 — 5d [1.5]°2	10	90
5210.5672	50	3p [1.5] 2 — 5d [3.5]°3	10	90
5222.3517	50	3p [2.5] 2 — 6s [1.5]°1	8	80
5326.3968	75	3p [0.5] 1 — 4d [1.5]°1	8	80
5330.7775	600	3p [0.5] 1 — 4d [1.5]°2	10	80
5341.0938	1000	3p [0.5] 1 — 4d [0.5]°1	10	90
5343.2834	600	3p [0.5] 1 — 4d [0.5]°0	8	90
5355.176	150	3p'[1.5] 2 — 5d [2.5]°3	7	90
5398.49			7	100
5399.48			40	100
5400.5616	2000	3s [1.5]°1 — 3p'[0.5] 0	500	100
5433.6513	250	3p [0.5] 1 — 5s'[0.5]°1	8	100
5448.5091	150	3p [0.5] 1 — 5s'[0.5]°0	7	100
5511.485	15	3p [2.5] 3 — 4d'[2.5]°3	8	100
5562.7662	500	3p [2.5] 2 — 4d'[2.5]°3	8	90
5748.650	70	3p [2.5] 3 — 4d [2.5]°2	8	60
5764.063	3	3p [2.5] 3 — 4d [3.5]°3	8	70
5764.4188	700	3p [2.5] 3 — 4d [3.5]°4	10	70

Table 1—*continued.*

Wavelength in Air(Å)	Intensity of Emission	Ne Transition	OG Signal Intensity(mV)	Laser Energy (μJ)
5770.307	50	3p'[0.5] 0 — 5d'[1.5]°1	3	80
5804.4496	500	3p [2.5] 2 — 4d [2.5]°2	3	90
5820.1558	500	3p [2.5] 2 — 4d [3.5]°3	4	100
5881.8950	1000	3s [1.5]°2 — 3p'[0.5] 1	3800	90
5902.4623	50	3p'[1.5] 2 — 4d'[2.5]°3	4	80
5944.8342	500	3s [1.5]°2 — 3p'[1.5] 2	2300	50
5965.4710	500	3p'[0.5] 1 — 4d'[1.5]°2	4	40
5975.5340	600	3s [1.5]°2 — 3p'[1.5] 1	1300	40

seen that the pulse shapes are quite different. The waveform in Fig. 3(a) corresponds to the neon transition $3s[1.5]^0 2$–$4p[0.5]1$ at 3510.721 Å. It is a negative peak with a 17 μsec. full-width at half-maximum (FWHM) that rises and changes polarity to become a positive peak with a 100 μsec. FWHM. The waveform shown in Fig. 3(b) refers to the neon transition $3s[1.5]^0 1$–$4p[2.5]2$ located at 3515.190 Å that is oscillatory in nature. It has two negative peaks with FWHM of about 8 and 117 μsec. and a positive peak with a 13 μsec. FWHM in between. The waveform illustrated in Fig. 3(c) represents the neon transition $3s'[0.5]^0 1$–$4p'[0.5]0$ at 3520.471 Å and is an initially negative-going peak about 23 μsec. FWHM that decays gradually over 225 μsec. into more or less a flat tail. Figures 4(a) and (b) show two OG waveforms of the same neon transition $3s[1.5]^0 2$–$4p[0.5]1$ at 3510.721 Å recorded with two different discharge currents 1.00 and 0.25 mA respectively. The pulse shape shown in Fig. 4(b) was recorded with a discharge current of 0.25 mA and has a wider pulse-width of 19 μsec. FWHM compared to the pulse shown in Fig. 4(a) for 1.00 mA that had a pulse-width of 15 μsec. Despite the two waveforms having similar overall shapes their positive portions are different, in

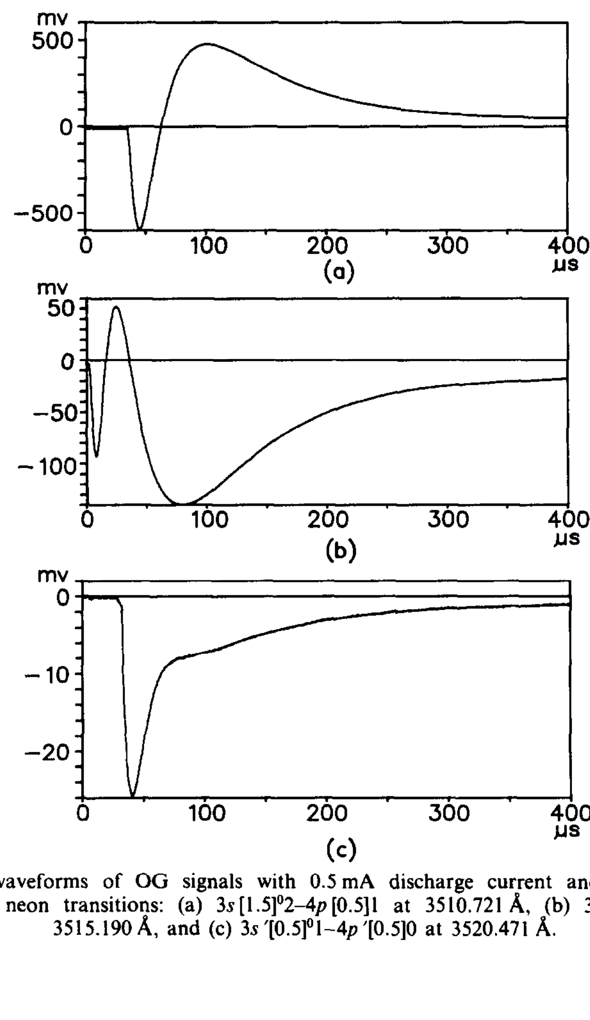

Fig. 3. Sample waveforms of OG signals with 0.5 mA discharge current and 20 μJ laser pulse corresponding to neon transitions: (a) $3s[1.5]^0 2$–$4p[0.5]1$ at 3510.721 Å, (b) $3s[1.5]^0 1$–$4p[2.5]2$ at 3515.190 Å, and (c) $3s'[0.5]^0 1$–$4p'[0.5]0$ at 3520.471 Å.

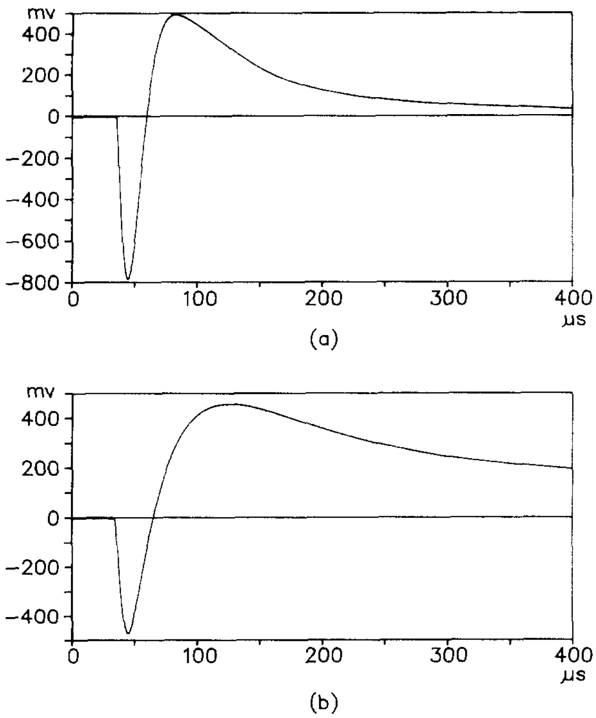

Fig. 4. Waveforms of the OG signal from neon transition $3s[1.5]^o2$ – $4p[0.5]1$ at 3510.721 Å using a 20 µJ laser pulse and discharge current (a) 1.00 mA and (b) 0.25 mA.

that the higher current pulse is narrower, almost a third as wide as compared to the pulse recorded with the smaller discharge current. While recording the OG spectra special attention has to be paid in positioning the gate of the boxcar. The position of the gate changes the intensity and polarity of the signals. The intensities of the OG transitions listed in Table 1 correspond to the absolute amplitudes at the peak of the pulse.

A detailed discussion of the time evolution of the OG signals has been given by Smyth and Schenck,[20] and by Reddy et al.[23] Theoretical approaches to explain the OG phenomena have been carried out by Erez et al.[24] van Veldhuizen et al,[25] and Stewart et al.[26] Our present investigations have been confined to a systematic and comprehensive identification and tabulation of laser-induced OG transitions in the u.v. and visible regions of the electromagnetic spectrum so as to calibrate the wavelengths of tunable lasers to within $0.3\ cm^{-1}$ accuracy. No attempts have been made to explain the intensities and the temporal behavior of the OG signals.

The wavelength position between OG transitions can be determined by counting the simultaneously recorded interference fringes. The free spectral range of the etalon can be simply determined by dividing the wavenumber difference between OG transitions by the number of fringes in-between. For example, in Fig. 2, the wavenumber for position P is given by:

$$N_P = N_A + K_{PA}(N_B - N_A)/K_{BA} \qquad (1)$$

where N_P, N_A and N_B are the wavenumbers at positions P, A and B, respectively, and K_{PA} and K_{BA} are the number of fringes between A and P, and between A and B, respectively. The nonlinearity of the refractive index of quartz, $\sim 10^{-6}$/nm in the blue region, can be ignored because the linewidth of the OG signals was typically $0.3\ cm^{-1}$ for the spectra recorded using an average over 10 shots for each data point. For instance, with $N_A = 28553.33\ cm^{-1}$, $N_B = 28579.06\ cm^{-1}$ and $K_{BA} = 53.7$ and $K_{PA} = 15.9$, the formula represented by Eq. (1) yields for the position P a value of $28560.95\ cm^{-1}$.

In summary, we have recorded 351 optogalvanic transitions using a commercial iron neon hollow cathode discharge lamp, and of which 223 lines have been assigned to neon transitions in the 337–598 nm region. To the best of our knowledge, most of these laser-assisted OG lines are being reported here for the first time and should be very useful for precise wavelength calibration.

An observation of the OG signal, along with simultaneous recording of interference fringes from an etalon, has provided precise and reliable calibration of laser-induced fluorescence excitation spectra of jet-cooled free radicals.

Acknowledgements—This work was supported by the U.S. Environmental Protection Agency (Grant No. R819720-01-0), the Collaborative Core Unit of Howard University's Graduate School of Arts & Sciences, and the National Aeronautics and Space Administration Center for the Study of Terrestrial and Extraterrestrial Atmospheres (Grant No. NASA NAGW-2950).

REFERENCES

1. S. Gerstenkorn et P. Luc, "Atlas du Spectre D'absorption de la Molecule D'iode", Editions du Centre National de la Recherche Scientifique, Paris (1978).
2. T. -Y. D. Lin, X. -Q. Tan, T. M. Cerny, J. M. Williamson, D. W. Cullin, and T. A. Miller, *Chem. Phys.* **167,** 203 (1992).
3. F. M. Penning, *Physica* **8,** 137 (1928).
4. R. B. Green, R. A. Keller, G. G. Luther, P. K. Schenck, and J. C. Travis, *Appl. Phys. Lett.* **29,** 727 (1976).
5. R. A. Keller, R. Engelman Jr., and B. A. Palmer, *Appl. Opt.* **19,** 836 (1980).
6. N. J. Dovichi, D. S. Moore, and R. A. Keller, *Appl. Opt.* **21,** 1468 (1982).
7. B. M. Suri, R. Kapoor, G. D. Saksena, and P. R. K. Rao, *Opt. Commun.* **49,** 29 (1984).
8. B. M. Suri, R. Kapoor, G. D. Saksena, and P. R. K. Rao, *Opt. Commun.* **52,** 315 (1985).
9. F. Babin, P. Camus, J. -M. Gagne, P. Pillet, and J. Boulmer, *Opt. Lett.* **12,** 468 (1987).
10. D. S. King, P. K. Schenck, K. C. Smyth, and J. C. Travis, *Appl. Opt.* **16,** 2617 (1977).
11. M. H. Begemann and R. J. Saykally, *Opt. Commun.* **40,** 277 (1982).
12. A. Rosenfeld, S. Mory, and R. Konig, *Opt. Commun.* **30,** 394 (1979).
13. J. R. Nestor, *Appl. Optics* **21,** 4154 (1982).
14. V. M. Gusev and O. N. Kompanets, *Sov. J. Quantum Electron.* **17,** 1515 (1978).
15. B. R. Reddy, P. Venkateswarlu, and M. C. George, *Opt. Commun.* **75,** 267 (1990).
16. M. Duncan and R. Devonshire, *Inst. Phys. Conf. Ser. No.* **113:** Section 6, 207 (1990).
17. M. -C. Su, S. R. Ortiz, and D. L. Monts, *Opt. Commun.* **61,** 257 (1987).
18. Y. Oki, T. Izuha, M. Maeda, C. Honda, Y. Hasegawa, H. Futami, J. Izumi, and K. Matsuda, *Jap. J. appl. Phys.* **30,** L1744 (1991).
19. M. Hippler and J. Pfab, *Opt. Commun.* **97,** 347 (1993).
20. K. C. Smyth and P. K. Schenck, *Chem. Phys. Lett.* **55,** 466 (1978).
21. A. R. Striganov and N. S. Sventitskii, "Table of Spectral Lines of Neutral and Ionized Atoms", Translated from Russian, IFI/Plenum, New York, NY (1968).
22. G. Racah, *Phys. Rev.* **61,** 537 (1992).
23. B. R. Reddy, P. Vekateswarlu, and M. C. George, *Opt. Commun.* **73,** 117 (1989).
24. G. Erez, S. Lavi, and E. Miron, *IEEE J. Quantum Electron.* **QE-15,** 1328 (1979).
25. E. M. van Veldhuizen, F. J. de Hoog, and D. C. Schram, *J. appl. Phys.* **56,** 2047 (1984).
26. R. S. Stewart, K. W. McKnight, and K. I. Hamad, *J. Phys. D: Appl. Phys.* **23,** 832 (1990).